Lasers in Manufacturing Conference 2017

Nucleate boiling in laser beam welding of aluminum alloys

Florian Hugger[a,*], Matthias Holzer[b], Stephan Roth[b,d] , Michael Schmidt[b,c,d]

[a]*BBW Lasertechnik GmbH, Gewerbering 11, 83134 Prutting, Germany*
[b]*Bayerisches Laserzentrum GmbH (blz), Konrad-Zuse-Straße 2-6, 91052 Erlangen, Germany*
[c]*Institute of Photonic Technologies (LPT), Friedrich-Alexander-Universität Erlangen-Nürnberg, Konrad-Zuse-Straße 3-5, 91052 Erlangen, Germany*
[d]*Erlangen Graduate School in Advanced Optical Technologies (SAOT), Paul Gordan Straße 6, 91052 Erlangen, Germany*

Abstract

Aluminum alloys with high magnesium and zinc content are hard to weld due to severe spatter formation and welding defects. To understand the physical mechanism of spatter formation a spot welding process is observed by high speed imaging. The analysis of the videos with a frame rate of 240,000 fps shows a new phenomenon. Bubbles are generated below the surface which expand and erupt. When collapsing the thin melt film which formed the shell of the bubble disintegrates to spatters. The dynamics of bubble movement and the collapse of the melt film into spatter droplets are described.
Moreover a mechanism for the bubble generation is proposed. Due to selective evaporation of volatile alloying elements, the concentration of alloying elements at the evaporating surface is reduced. In consequence of diffusion of alloying elements towards the evaporating surface, these elements are reduced in the upper surface layers. Due to the change of element concentration, the evaporation temperature of the surface and the subjacent melt layers can increase. When the evaporation temperature is lower than the real temperature in the melt layers below the surface, a vapor nucleus is generated. The depth of nucleus formation and the pressure inside a bubble are calculated.

Keywords: Welding, boiling, bubbles

* Corresponding author. Tel.: +49-8036-9082-065 ; fax: +49-8036-9082-028 .
E-mail address: f.hugger@bbw-lasertechnik.de .

1. Introduction

In laser beam welding spatter formation is a severe problem, since material is lost and the optics can be contaminated. In Kaplan, 2010 a summary of different mechanisms of spatter formation is given. In this paper a new mechanism is presented and described.

The mechanism is based on bubble formation and is only observed in alloys with alloy elements of low boiling point. Moreover the time scale for the evolution and the collapse of a bubble is usually below 20 µs which makes it difficult to investigate.

2. Experimental setup

Therefore the laser welding process is recorded with a high speed camera with a frame rate of 240,000 frames per second, which results in a time between images of 4.2 µs. For the experimental investigations a 6 kW disk laser is used for bead on plate weld. The laser beam is deflected and focused to a spot diameter of 170 µm by a scanner optic. Since the resulting keyhole diameter of about 200 µm is hard to observe, the laser beam is defocused by 7 mm so that a spot diameter of 680 µm on the sheet surface results. The high speed camera is oriented to the welding process in an angle of 30° to the laser beam axis, see Fig. 1. To investigate both conduction mode welding and deep penetration welding, the laser power is linearly increased from 0 kW to 4 kW within 300 ms and then switched off.

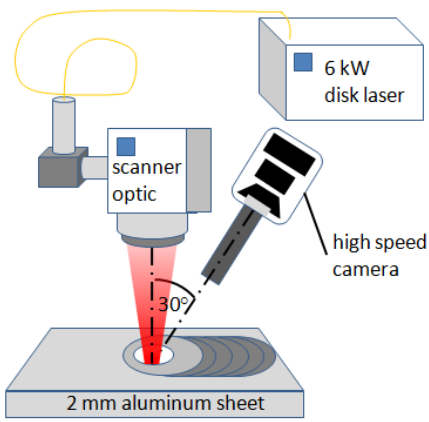

Fig. 1. Schematic of experimental setup

Different aluminum alloys with increasing amount of volatile alloying elements are used in the experiments: AlMg1, AlMg3, AlMg4.5Mn and AlZn5.5MgCu. All alloys have a sheet thickness of 2 mm. The formation of bubbles can be observed in all investigated materials. Nevertheless the bubble eruptions, which are accompanied by spatter formation, are more intensive and frequent in high alloyed aluminum. Therefore most of the following investigations are carried out with AlMg1, where the bubble formation can be studied best. The bubbles occur inside as well as at the rim of the keyhole. Due to vapor and spatters, the quality of the images inside the capillary is low. Therefore most displayed bubbles are at the rim of the vapor capillary.

3. Results and discussion

At first the evolution and collapse sequence of a bubble are shown, followed by characteristic images of erupting bubbles. After this spatter generation is displayed and a mechanism of the bubbles formation is proposed. Finally the pressure inside a bubble is estimated.

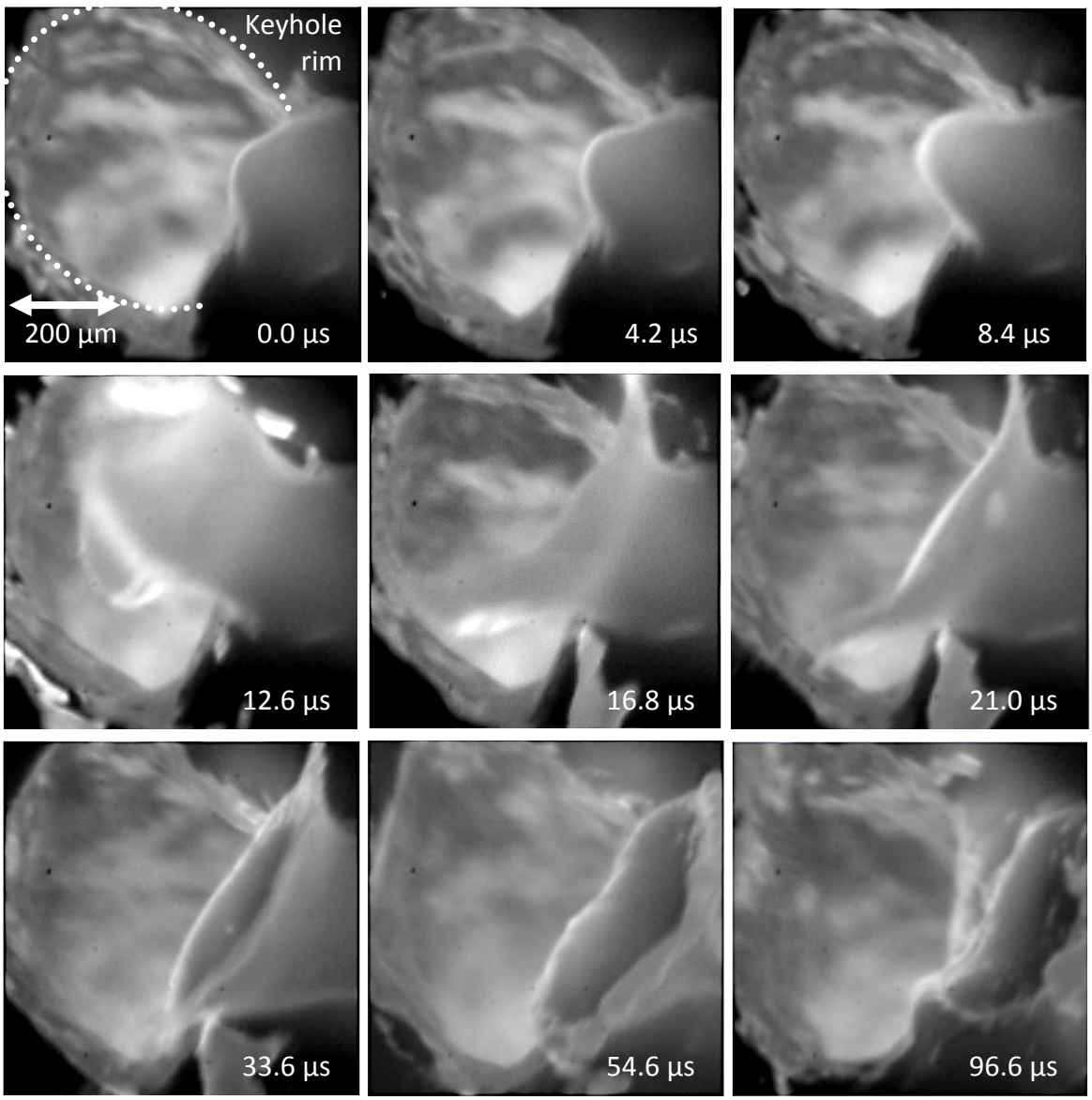

Fig. 2. Formation and collapse in side view of a bubble for AlMg1

3.1. Formation and collapse of bubbles

In Fig. 2 and 3 the formation sequences of two different bubbles are displayed. Fig. 2 shows an evolution in side view, while in Fig. 3 a front view of a bubble is displayed.

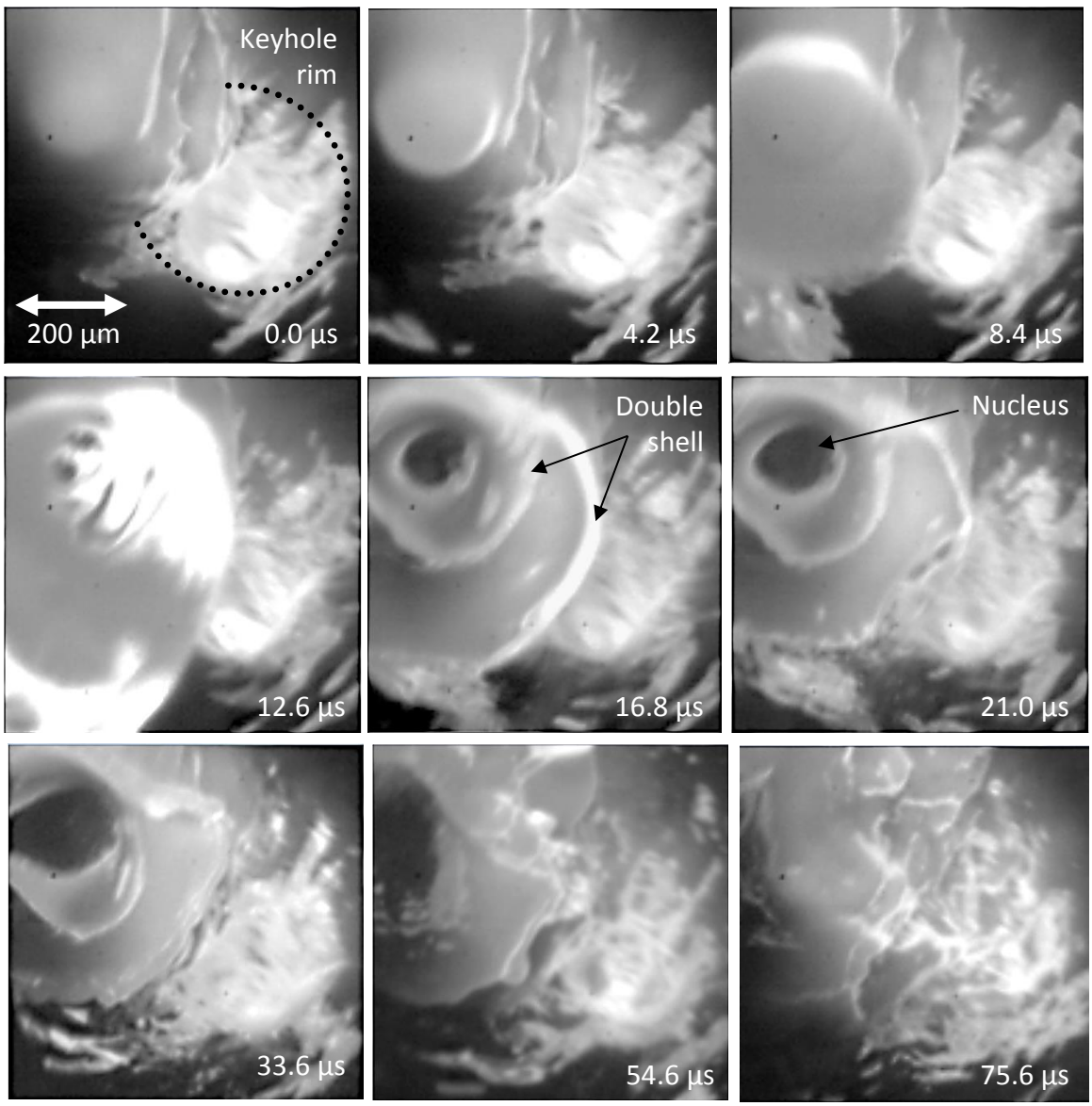

Fig. 3. Formation and collapse of a bubble in front view for AlMg1

At the beginning a hump is formed which grows from the surface of the melt to a bubble. The bubble expands until 12.6 µs. Here the bubble tears at the tip of the shell (see also Fig. 4a). The shell is driven sideways and reveals a double-shell structure surrounding a dark cavity in the centre of the bubble, see Fig. 3 at 16.8 µs. Finally, the shell collapses and looses its shape. The shell is retraced until only a small crater is visible which vanishes after 100 µs.

The time scale of over 75 µs of the sequences is not typical since the bubble formation and collapse usually elapse within 10-20 µs. But to show and explain all phases in one sequence very slowly developing bubbles are chosen.

To give a better insight into the different shapes of bubbles, Fig. 4 shows an overview of bubble formation for different alloys, positions and welding modes. Bubbles form from a growing hump at the surface and expand until the shell tears. In Fig. 4a the moment of tearing is displayed. After tearing the shell is retraced and the inner structure of the bubble is visible. The structure is principally similar for all investigated alloys, Fig. 4b and 4c. In high alloyed aluminum often multi-eruptions take place, which means that several eruptions occur in one position at one time. Fig. 4d displays a multi-eruption with four nuclei.

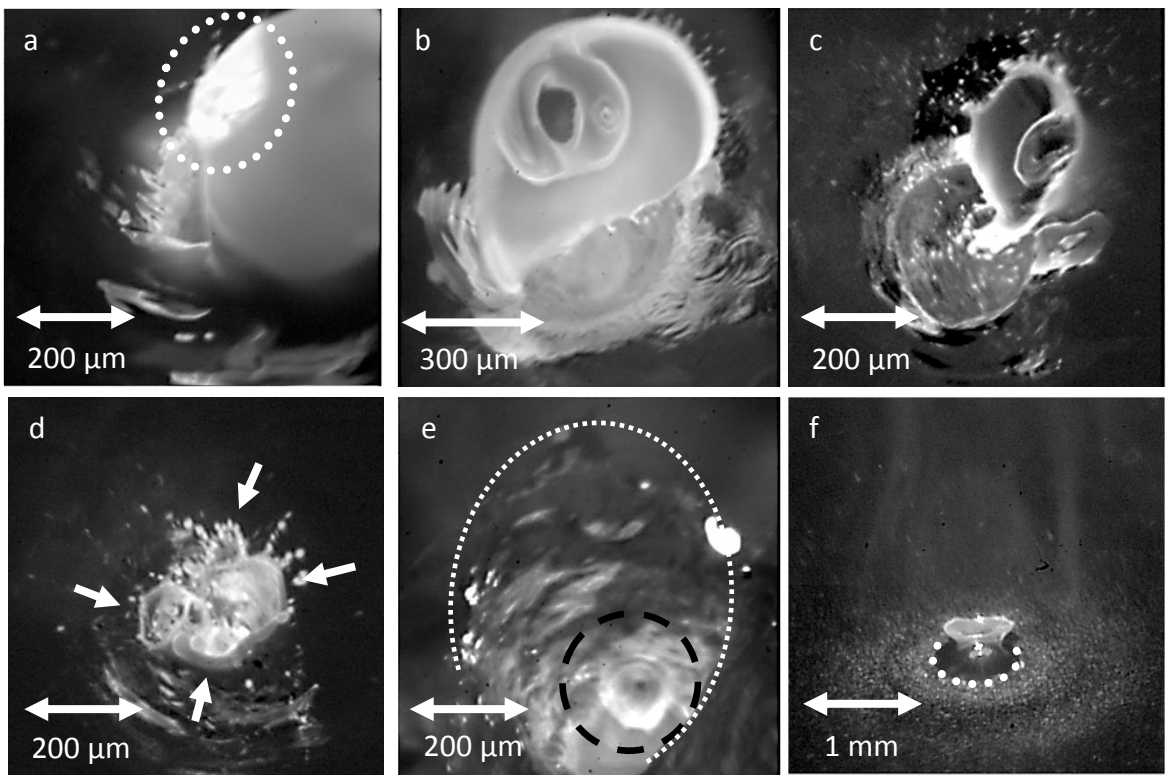

Fig. 4. Characteristic images of bubble eruption
(a) at the moment of eruption for AlMg1
(b) at the rim of the keyhole for AlMg1
(c) at the rim of the keyhole for AlZn5,5MgCu
(d) with multi nucleus eruptions for AlZn5,5MgCu
(e) inside the keyhole during seam welding in AlMg1 with 3.5 kW and 25 mm/s
(f) in conduction mode welding for AlZn5,5MgCu after melt pool formation observed from an angle 60° to the laser beam axis

In this paper, most of the images of nucleate boiling are taken from a spot welding process, but bubble formation also takes place in seam welding and inside the keyhole, Fig. 4e. In Fig. 4e the rim of the keyhole is marked with a white dashed line. Moreover, the boiling phenomenon can be observed in conduction mode welding. Fig. 4f shows an eruption from a small melt pool (marked with white dashed line) before keyhole formation. The tearing bubble almost has the dimension of the weld pool. In Fig. 4b and Fig. 4c the inner structure of a bubble is visible. It shows a dark cavity in the center which is expected to be the nucleus of the bubble. It is surrounded by a first shell which itself is surrounded by second shell. From the formation sequence shown in Fig. 2 and Fig. 3 and the double-shell structure, the following evolution of a bubble is proposed which is schematically displayed in Fig. 5.

In a first stage a nucleus is generated below the melt surface (Fig. 5a). The mechanism of nucleus generation is detailed in section 3.3. The nucleus moves towards the melt surface and breaks though the surface (Fig. 5b). Here the nucleus is still covered by melt which is visible as a hump at the melt surface (see also Fig. 2 at 8.4 µs). The nucleus is rising and a bubble is formed (Fig. 5c). The bubble expands in direction away from the melt since the melt film covering the nucleus gets thinner and cannot counteract the pressure of the nucleus (Fig. 5d). The expansion of the bubble is always one-sided, since the melt film is only thinned out at the opposite side of the melt. When the melt film is too thin, the shell tears (Fig. 5e) and the pressure inside the bubble can escape. The ruptured shell moves sidewards which leads to the double-shell structure with the inner and outer shell (Fig. 5f). Afterwards both shells are retraced and finally disappear in the melt (Fig. 5g-i).

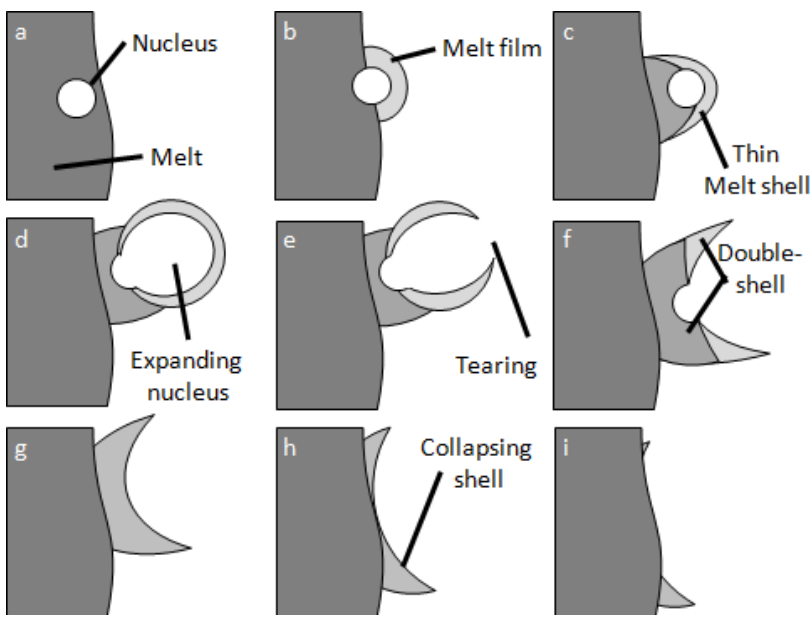

Fig. 5. Schematic of bubble formation sequence

3.2. Formation of spatters

It can be observed that the tearing of bubbles leads to the formation of small spatters. The generation of spatters is much more frequent in high alloyed aluminum. The reasons for this observation are not clear up to now. Nevertheless, the mechanism is expected to be the same for all alloys.

The formation of spatters is displayed in the sequence in Fig. 6. A hump is generated and expands to a bubble (0.0 µs). The bubble expands and erupts after 4.2 µs. The image after 8.4 µs shows the outer shell of the ruptured bubble. In the following images, it can be observed that the shell is disintegrating from a continuous surface (8.4 µs) into single jets (12.6 µs and 16.8 µs) and finally into small droplets (16.8 µs and 21 µs).

The melt film of the thin shell has a very high ratio of surface area to volume. For this reason it tries to decrease its surface area which leads first to the formation of melt jets and finally to the formation of small droplets. The droplets are small compared to spatter generated by other mechanisms described in Kaplan, 2010. The typical diameter is below 50 µm.

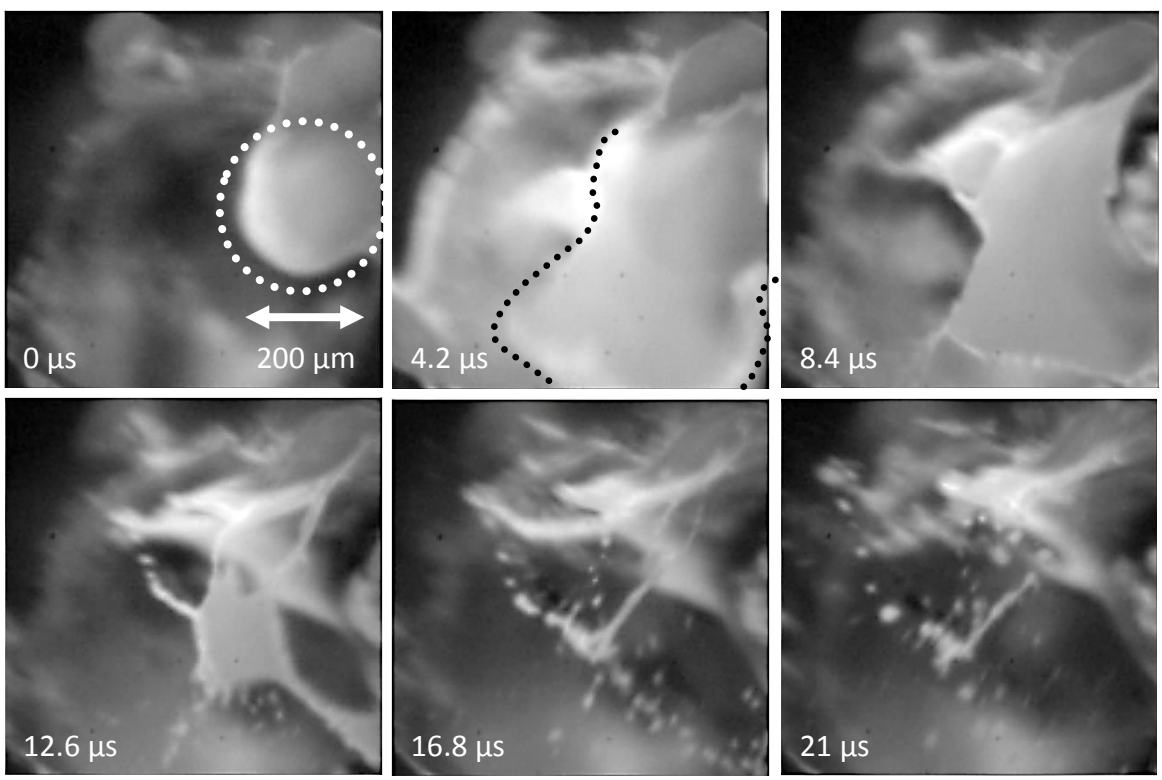

Fig. 6. Disintegration of the shell of a bubble into isolated spatters for AlMg3.

3.3. Theoretical model for vapor nucleus generation

Different mechanisms of nucleus generation have been considered. Since the eruptions can be observed deep inside the vapor capillary (Fig. 4e), an entrapment of atmospheric gases is ruled out. Furthermore vortices of metal vapor inside the capillary are refused as a probable reason, since eruptions of the melt pool

are observed also in conduction mode welding, when the evaporation and the vapor flow are in the same direction and originating from a flat surface (Fig. 4f). As a consequence, the nucleus for the bubble is most likely to be generated under the surface of the melt. To generate a vapor nucleus the evaporation temperature must be lower than the real temperature at a certain position below the melt surface.

A mechanism where the temperature for phase change is different from the real local temperature is known from constitutional supercooling. In constitutional supercooling, due to an inhomogeneous alloying element concentration at the solid-liquid interface, the real temperature is locally lower than the solidification temperature of the melt. As a consequence solidification nuclei are formed in the melt in some distance to the solidification front and an equiaxed or dedritical solidification structure develops (Kou, 2003). The same situation can occur at the liquid-vapor interface. When the boiling temperature is lower than the real temperature, the melt starts to evaporate and a nucleus is generated below the surface.

It is known from literature that differences of evaporation temperatures of base material and alloying elements result in a selective evaporation of alloying elements. If the evaporation temperature of the alloying element is lower than the evaporation temperature of the base material there is a loss of the alloying element in the melt, since its vapor pressure and therefore its evaporation rate is higher (Jandaghi, 2010).

As a consequence, since the evaporation rate at the surface is much faster than the diffusion rate of an alloying element towards the liquid-vapor interface, the composition of the melt at the surface changes. The alloying element concentration in the melt layers below the surface can be calculated. Since the calculations are extensive, they will be published in detail in a future paper and only the results are given here to provide a basis to understand the physical mechanism.

Though the evaporation rate of the alloying element at the surface is unknown, the rate was chosen in a way that the resulting relative loss of the alloying element in the melt pool is about 20 % as reported by Dilthey, 2000. The result for the aluminum alloy AlMg5, assuming a cylindrical keyhole and melt pool with a keyhole diameter of 1 mm and a melt pool diameter of 3 mm, is displayed in Fig. 7. It can be observed that there is a steep concentration gradient especially in the melt layers close to the surface (about 25 µm). The results are similar to those of Dilthey, 2000.

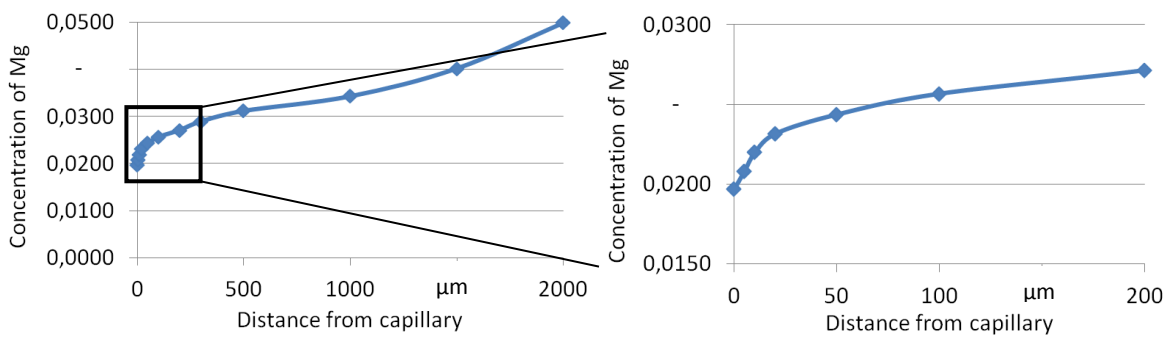

Fig. 7. Alloying element concentration as a function of distance from vapor capillary

Because of the composition change of the melt layers close to the surface the evaporation temperature of these layers increases. Fig. 8 shows the evaporation temperature (boiling curve) of the binary system Al-Mg. It can be observed that especially for a magnesium content of <10 % the evaporation temperature changes rapidly with alloy composition. The calculations are carried out similarly as described in Rapp, 1994.

With the results of the concentration dependent evaporation temperature and the concentration distribution of the alloying element in the melt pool close to the keyhole, the evaporation temperature distribution of the alloy below the surface can be calculated. The temperature distribution of the real

temperature can be calculated using the heat conduction equation, assuming a cylindrical keyhole and melt pool with a keyhole diameter of 1 mm and a melt pool diameter of 3 mm again. Fig. 9 shows the distribution of the real temperature and the evaporation temperature in the melt pool. It can be observed that the evaporation temperature is up to 20 °K below the real temperature in a distance 20 µm from the vapor capillary. Therefore, the criterion for the generation of a vapor nucleus is fulfilled in a distance <40 µm to the melt surface.

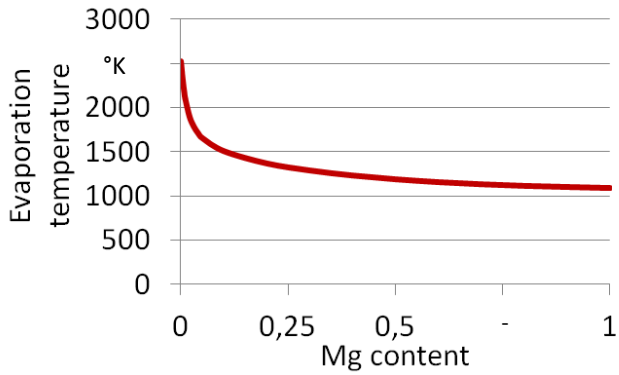

Fig. 8. Evaporation temperature of the binary system Al-Mg

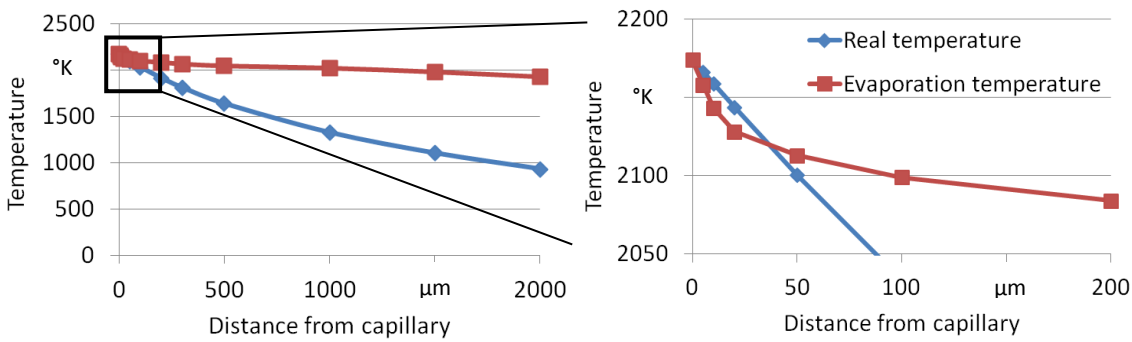

Fig. 9. Real and evaporation temperature as a function of distance from the vapor capillary

The calculations show that the idea of the generation of a vapor nucleus below the surface of the melt is sensible. Nevertheless the calculations are based on assumptions for material data close to evaporation temperature of aluminum, since accurate measurements are not available.

3.4. Pressure inside a bubble

As stated before the nucleus size of 100 µm is not representative. A measurement of the size of nuclei for different alloys is displayed in table 1. The measurements are carried out by determining the size of the nuclei in the images of the high speed camera videos in pixels. The pixels are correlated to millimeter scale by determining the melt pool diameter after the welding process.

The nuclei have an average diameter of about 35 µm. The investigations show that the alloy composition has no clear influence on nuclei size. The pressure inside a bubble is in equilibrium with the surface tension of the surrounding melt.

Table 1. Measurements of nucleus size of different aluminum alloys

Alloy	Average nucleus diameter (n=10)	Standard deviation
AlMg1	32,7 µm	10,1 µm
AlMg3	35,0 µm	11,6 µm
AlMg4,5Mn	32,3 µm	9,3 µm
AlZn5,5MgCu	41,4 µm	16,1 µm

From the radius of a nucleus and the surface tension of the melt the pressure inside the bubble can be estimated using the Young-Laplace-equation (Polifke, 2005):

$$p_V = p_0 + \frac{2\sigma_{ST}}{r_N} \approx 1.93\ bar \qquad (1)$$

In equation (1) p_V is the pressure inside the bubble, p_0 the atmospheric pressure, σ_{ST} the surface tension of AlMg5 at 973 °K with a value of 0.798 N/m (Goicoechea, 1992) and r_N the radius of an average nucleus (r_N=17,5 µm). This results in a pressure inside the bubble of about 1.93 bar. The surface tension of aluminum is lower at increased temperatures nearby the evaporation temperature. Therefore the real pressure inside the bubble is probably lower than the calculated pressure.

4. Conclusion and outlook

The observation of a welding process of aluminum alloys with magnesium and zinc content shows a new phenomenon which can be explained by nucleate boiling below the surface of the melt. Possible formation mechanisms of the bubble and the vapor nucleus are proposed. Calculations give a pressure inside the bubble of about 1.93 bar. Nevertheless, the formation mechanism is not yet fully understood. It is observed that the eruptions are more often and more intense in high alloyed aluminum, but the nucleus size is similar. Therefore it is suggested that the generation depth of the nucleus is different and also the surface tension of different alloys has significant influence. In a following paper more observations from nucleate boiling and its impact on the keyhole geometry will be presented. Moreover a detailed calculation of the evaporation temperature distribution below the melt surface for different aluminum alloys will be given.

References

Dilthey, U., Goumeniouk, A., Lopota, V., Turichin, G., Valdaitseva, E., 2000. Development of a theory for alloying element losses during laser beam welding, Journal of Physics D: Applied Physics 34, p.81.

Goicoechea, J.,Garcia-Cordovilla, C., Louis, E., Pamies, A., 1992. Surface tension of binary and ternary alloys of the system Al-Si-Mg and Al-Zn-Mg, Journal of Materials Science 27, p.5247.

Jandaghi, M., Parvin, P., Torkamany, M. J., Sabbaghezadeh, J., 2010. Alloying element change of SS-316 and Al-5754 during laser welding unsing real tme laser induced breakdown spectroscopy (LIBS) accompanied by EDX and PIXE microanalysis, Physics Proceedia 5, p. 107.

Kaplan, A. F. H., Powell, J., 2010. “Laser welding:The spatter map, “ 29th International Congress on Applications of Laser & Electro-optics, USA, paper 1906.

Kou, S., 2003. Welding metalurgy. John Wiley & Sons, Inc., Hoboke, New Jersey.

Polifke, W., Kopitz, J., 2005. Wärmeübertragung: Grundlagen, analyitsche und numerische Methoden, Pearson Education, München.

Rapp, J., Beck, M., Dausinger, F., Hügel, H., 1994. Fundamental approach to the laser weldability of aluminium- and copper-alloys, 5th European Conference on Laser Treatment of Materials, p. 313.